Real-time Probabilistic Reachability Forecasting for Gliders in the Gulf of Mexico

E.M. Mule[a], P.J. Haley, Jr.[a], C. Mirabito[a], S.F. DiMarco[b], S. Mahmud[b], A. Dancer[b], X. Ge[b], A.H. Knap[b], Y. Liu[b],
U.C. Nwankwo[b], S. Glenn[c], T.N. Miles[c], D. Aragon[c], K. Coleman[c], M. Smith[c], M. Leber[d], R. Ramos[d],
J. Storie[d], G. Stuart[e], J. Marble[e], P. Barros[e], E.P. Chassignet[f], A. Bower[g], H.H. Furey[g], B. Jaimes de la Cruz[h],
L.K. Shay[h], M. Tenreiro[i], E. Pallas Sanz[i], J. Sheinbaum[i], P. Perez-Brunius[i], D. Wilson[j], J. van Smirren[k],
R. Monreal-Jiménez[l], D.A. Salas-de-León[l], V.K. Contreras Tereza[m], M. Feldman[n], M. Khadka[n], and
P.F.J. Lermusiaux[a,†]

[a]*Department of Mechanical Engineering, Massachusetts Institute of Technology, Cambridge, MA*
[b]*Department of Oceanography, Texas A&M University*, [c]*Department of Marine and Coastal Sciences, Rutgers University*
[d]*Woods Hole Group, Inc.*, [e]*Fugro*, [f]*Department of Earth, Ocean and Atmospheric Science, Florida State University*
[g]*Physical Oceanography, Woods Hole Oceanographic Institution*
[h]*Rosenstiel School of Marine, Atmospheric, and Earth Science, University of Miami*
[i]*Department of Oceanography, CICESE*, [j]*University of the Virgin Islands*, [k]*Ocean Sierra*
[l]*Universidad Nacional Autónoma de México*, [m]*Mexican Institute of Water Technology*, [n]*Gulf Research Program, NASEM*
[†]Corresponding author: pierrel@mit.edu

Abstract—As part of the Mini-Adaptive Sampling Test Run (MASTR) experiment in the Gulf of Mexico (GoM) region from February to April 2024, we demonstrated real-time deterministic and probabilistic reachability analysis and time-optimal path planning to guide a fleet of four ocean gliders. The governing differential equations for reachability analysis and time-optimal path planning were numerically integrated in real-time and forced by currents from our large-ensemble ocean forecasts. We illustrate the real-time deterministic and probabilistic forward reachability analyses, reachability and path planning for glider pickups, time-optimal path planning for gliders in distress, and planning of future glider deployments. Results show that the actual paths of gliders were contained within our reachable set forecasts and in accord with the dynamic reachability fronts. Our time-optimal headings and paths also predicted real glider motions, even for longer-range predictions of weeks to a month duration. Reachability and time-optimal path planning forecasts were successfully employed for glider recovery. They also enabled exploring options for future glider deployments.

Index Terms—Ocean forecasting, sea glider, path planning, reachability analysis, probabilistic forecasting, adaptive sampling.

I. INTRODUCTION

Optimal path planning for autonomous marine vehicles has made major advances in the past decade [1–10]. Remote control operations of these marine vehicles is common, from vertical actuation with autonomous profiling floats to three-dimensional motions with gliders and other underwater vehicles [11–20]. Progress has been made with ocean gliders and their operations in longer-term missions [21–29] leading to a growing body of expertise and best practices [30–32]. However, due to the highly dynamic and uncertain ocean currents [33, 34], the various hazards and biofouling [35, 36], and the limited vehicle power, propulsion speeds, and communication [17, 37–40], model-based planning for longer-range endurance missions at scales much larger than these of the vehicles remains challenging. Principled planning theory and schemes fully integrating data-assimilative model predictions and control theory are not often used in real-time with autonomous underwater vehicles (AUVs) at sea [6]. To our best knowledge, it is only recently that four-dimensional optimal control differential field equations forced with forecasts from four-dimensional ocean modeling systems were used to directly control vehicles in real-time at-sea experiments. In 2016, AUVs used forecast time-series of headings computed by time-optimal path planning differential equations forced by ocean current forecasts in a complex coastal region. The AUVs that followed the forecast time-optimal headings reached their targets first, winning all races, even though they travelled longer distances than other AUVs [41]. Differential reachability forecasts were also issued for real floats and gliders during the Northern Arabian Sea Circulation-Autonomous Research (NASCar) experiment [42, 43]. The utilization of such path planning and reachability analysis holds much promise for multiple scientific and societal applications, from offshore energy, fishing industry, transport, tourism, and security, to climate, weather, ocean, and hurricane monitoring and forecasting, and many other applications [6, 17, 31, 44, 45].

In this work, we employ the MIT-MSEAS (Multidisciplinary Simulation, Estimation, and Assimilation Systems) path planning theory and schemes [6, 46]. We demonstrate the use of differential reachability analysis and time-optimal path planning forecasts to help guide a fleet of four ocean gliders in the Gulf of Mexico (GoM) region for more than two months. This real-time effort was part of the Understanding Gulf Ocean Systems (UGOS) program of the U.S. National Academies of Sciences, Engineering, and Medicine.

The collaborative sea experiment, the Mini-Adaptive Sampling Test Run (MASTR), occurred from February to April 2024 [47]. Using the MIT-MSEAS data-assimilative Primitive-Equation (PE) submesoscale-to-regional-scale ocean-modeling system [48–50], we issued daily deterministic and probabilistic forecasts of ocean fields and derived quantities in real-time [47, 51]. For three months, we provided multi-resolution

ensemble forecasts. They were forced with stochastic tides and air-sea fluxes and initialized by downscaling from two global models with 3D PE-field perturbations using Error Subspace Statistical Estimation (ESSE) and stochastic forcing [50, 52–54]. We issued mutual information forecasts, optimal adaptive sampling guidance for air and sea platforms, and reachability and path planning forecasts for underwater vehicles. The latter were used by four gliders that sampled the western Caribbean Sea including the Yucatan Current and the mesoscale eddies in the region, clearly showing the presence of subsurface salinity maxima. The data was processed, quality-controlled, and assimilated in real-time [47].

Because ocean gliders are relatively slow (0.3–0.5 m/s) with respect to the prevailing currents (upwards of 1 m/s in portions of the Yucatan Current), it can be difficult to intuitively predict what areas are accessible to the gliders and what trajectories are time-optimal. Examples of common questions that glider operators ask include: Can my glider reach this location in the coming days? Which glider could go in this region and provide ideal measurements of specific ocean features? How can the gliders best avoid or best leverage the strong current regions? A glider had some damage and his nominal propulsion and dive patterns are altered, can it still reach the original locations or these new locations? Could it be picked up in this region? To plan our glider operations for next year, what is feasible and what are ideal drop-off locations to reach our scientific or operational goals? To quantitatively answer these questions, we built upon our rigorous level set differential equations [6, 55] to compute exact reachability fields and time-optimal paths for glider operations, given the uncertain future currents. These input currents and their probabilities were the real-time forecasts of the MSEAS-PE system.

In what follows, in section II, we describe the methodology for reachability analyses and time-optimal path planning. In section III, we present some of the real-time applications and results of our theory and schemes with the four MASTR gliders. We exemplify some of our deterministic and probabilistic forward reachability analyses, reachability and path planning for glider pickup, time-optimal path planning for gliders in distress, and planning of future glider deployments. Finally, we conclude in section IV.

II. Methodology

For our MASTR effort, the canonical reachability analysis and path planning consist of predicting the locations that a glider can reach as a function of time and the optimal paths to its desired locations, all of which depend on the ocean currents. Next, we introduce the notation and terminology, provide the governing differential equations and computational schemes that enable such predictions, and finally summarize the ocean modeling system and glider parameters.

A. Notation and Governing Equations

Along its path, a glider is advected by the ocean currents and we denote the current fields by $V(x, t)$ where x is the spatial location and t is time. For now, we assume that these ocean currents are deterministic. The ocean glider navigates from a given start location x_s at initial time $t_s = 0$ to a desired final location x_f. The position of the glider at time t is denoted by $X_p(t)$. During its mission, the glider has two main propulsion controls along its path, (i) its time-dependent nominal propulsion speed $F(t) \in [0, F_{\max}]$ where $F_{\max}$ is the maximum or desired cruising speed, and (ii) its time-dependent heading direction denoted by the unit vector $\hat{h}(t)$. For our application, the spatiotemporal scales of the ocean currents and glider missions (tens to hundreds of km, hours to days) are much larger than the glider scales (meters, seconds for the local controller). For our mission planning, we thus assume that the glider is in mechanical equilibrium at all times and governed the kinematic ordinary differential equation that sums the advection by the ocean currents with the propulsion by the glider,

$$\frac{\mathrm{d}X_p}{\mathrm{d}t} = V(X_p(t), t) + F(t)\,\hat{h}(t) \qquad (1)$$

For a marine vehicle, the *reachable set* $\mathcal{R}(x_s, t)$ is the set of physical locations in the ocean that can be reached at a time t when starting from an initial location x_s at time t_s and using operationally feasible speeds and headings, the vehicle controls. Without loss of generality, we can set $t_s = 0$. The *reachability front* $\partial\mathcal{R}(x_s, t)$ is the boundary of the reachable set. It is the furthest locations in the physical ocean space that the marine vehicle can reach at a given time t if it starts at x_s at t_s. Once this reachability front $\partial\mathcal{R}$ first reaches the desired final location x_f at some time t_f, a point that remained on $\partial\mathcal{R}$ and reached x_f corresponds to at least one *time-optimal path*. We can thus expect that such time-optimal paths can be computed by evolving a trajectory backward in time from x_f back to x_s.

Mathematically, to represent the reachable set and reachability front, we introduce a scalar value function $\phi(x, t)$ [6, 46, 56, 57]. The reachability front $\partial\mathcal{R}$ is a level set of this function (locations with a constant ϕ value or an isochrone). Without loss of generality, we can set this constant to be zero: the reachability front is then the zero level surface of ϕ. It is implicitly defined as all of the points x at time t where $\phi(x, t) = 0$. Initially, the reachability front is the start location x_s. As time advances, the reachability set and front expand due to the propulsion term $F(t)\,\hat{h}(t)$. Hence, we define the reachable set $\mathcal{R}$ as the set of locations where $\phi(x, t)$ is negative (inside the front $\partial\mathcal{R}$) or zero (at the front $\partial\mathcal{R}$).

As derived in [58, 59], for suitable Lipschitz conditions, the optimal evolution of $\phi(x, t)$ is governed by the Hamilton-Jacobi-Bellman (HJB) partial differential equation (PDE):

$$\frac{\partial\phi(x, t)}{\partial t} + F_{\max}\left\|\frac{\partial\phi}{\partial x}\right\| + V(x, t) \cdot \frac{\partial\phi}{\partial x} = 0$$

$$\phi(x, t = 0) = \phi_0 \qquad (2)$$

where $\frac{\partial\phi}{\partial x}$ denotes the generalized spatial gradient vector. To obtain this equation, the two controls $F(t)$ and $\hat{h}(t)$ are optimized using a control maximization principle and the fact that the propulsion speed is bounded by $F_{\max}$. The optimization results are the time-optimal control speed, $F^*(x, t) := F_{\max}$

2

(always travel at maximum cruising speed), and the time-optimal headings, $\hat{\boldsymbol{h}}^*(\boldsymbol{x},t) := \frac{\partial\phi}{\partial\boldsymbol{x}}\big|_{(\boldsymbol{x},t)} \left\|\frac{\partial\phi}{\partial\boldsymbol{x}}\big|_{(\boldsymbol{x},t)}\right\|^{-1}$ (always travel in the direction normal to the reachability front). Solving the PDE (2) for $\phi(\boldsymbol{x},t)$ provides the reachable set $\mathcal{R}(\boldsymbol{x}_s,t)$ and reachability front $\partial\mathcal{R}(\boldsymbol{x}_s,t)$: the latter is the zero level set of ϕ at any given time. In general, the PDE (2) is solved until the first time the reachability front reaches the final destination, i.e., until the time t_f such that $\phi(\boldsymbol{x}_f,t_f) = 0$. If this condition does not occur after some time, it implies that the desired final location is not reachable by that time.

Finally, starting from $\boldsymbol{x}_f$ at t_f, the optimal path is determined by solving the ODE (1) backward in time, using the optimal control $F^*(\boldsymbol{x},t) = F_{\max}$ and $\hat{\boldsymbol{h}}^*(\boldsymbol{x},t)$ defined above.

Stochastic governing equations. In our real-time applications, we also predict the uncertainty in the ocean current fields [51] and utilize this uncertainty to provide probabilistic reachability and path planning forecasts. In such probabilistic predictions, the ocean currents are denoted as $\boldsymbol{V}(\boldsymbol{x},t;\omega)$ where ω represents a specific realization or event of the uncertain ocean evolution. The ocean currents and dynamics are then modeled as stochastic processes [34, 52, 60] and a particular dynamical ocean realization is a sample path. Other variables that depend on $\boldsymbol{V}(\boldsymbol{x},t;\omega)$ such as ϕ, $\mathcal{R}$, $\partial\mathcal{R}$, $\boldsymbol{X}_{\boldsymbol{p}}^*$, and $\hat{\boldsymbol{h}}^*$ that we introduced in the above then also become stochastic processes dependent on ω. Their governing equations are then stochastic differential equations. For more details on the stochastic reachability analysis and path planning theory and schemes, we refer to [6, 61, 62]. We issued and used such probabilistic forecasts in real-time during MASTR and they will be highlighted in Sect. III.

B. Computational Schemes

For the glider motions, the complete path planning as done in [27] uses the four-dimensional ocean currents fields $\boldsymbol{V}(\boldsymbol{x},t)$ along the yoyo patterns of the gliders in the vertical. In this work, we instead consider an effective two-dimensional spatial approximation where the gliders feel the vertically-averaged ocean currents over the depth of their dives [42, 63]. This choice also mimics how glider operators commonly plan their missions based on the vertically-averaged currents seen by their gliders, which facilitated the collaboration among researchers during the real-time experiment.

The PDE (2) that we employed in real-time [47] was thus a two-dimensional in space PDE where the currents $\boldsymbol{V}(\boldsymbol{x},t)$ are our MIT-MSEAS PE forecast of the time-dependent ocean current fields, integrated from 0 to 1000 m depth. We initialize $\phi(\boldsymbol{x},t)$ to the function $\phi_0(x)$, the signed distance function to a very small circle centered at the start location $\boldsymbol{x}_s$ with a radius of the order of the grid spacing, i.e.:

$$\phi_0(\boldsymbol{x}) = \begin{cases} d(\boldsymbol{x}) & \text{if } \boldsymbol{x} \text{ is outside the initial circle} \\ -d(\boldsymbol{x}) & \text{if } \boldsymbol{x} \text{ is inside the initial circle} \end{cases} \quad (3)$$

This initialization with a radius of a few grid spacing (e.g., one or two) enables evaluating gradients of ϕ at a desired order of accuracy. As in acoustic propagation [64, 65], the initial starter

solution from x_s to the edges of this very small circle can be obtained analytically or approximately using eqs. (1)–(2).

For the numerical integration of the PDE (2), we use a second-order Essentially Non-Oscillatory (ENO) scheme in space and a second-order scheme in time [55, 57, 59]. We note that the numerical grid and time-step used to integrate the PDE (2) does not need to be the same as that of the ocean modeling system used to compute $\boldsymbol{V}(\boldsymbol{x},t)$.

Once the forward reachability solution $\phi(\boldsymbol{x},t)$ has been computed until the reachability front has arrived at all of the desired destination locations or a maximum time has passed, the integration of the PDE (2) can stop. Considering one such desired final location $\boldsymbol{x}_f$, the first time t_f when $\phi(\boldsymbol{x}_f,t_f) = 0$ indicates that $\boldsymbol{x}_f$ can be reached by time t_f. A time-optimal trajectory and its optimal headings $\hat{\boldsymbol{h}}^*(\boldsymbol{x},t)$ can then be obtained by *backtracking* of the ODE (1). Specifically, the optimal path $\boldsymbol{X}_{\boldsymbol{p}}^*(t)$ is governed by,

$$\frac{\mathrm{d}\boldsymbol{X}_{\boldsymbol{p}}^*}{\mathrm{d}t} = -\boldsymbol{V}(\boldsymbol{X}_{\boldsymbol{p}}^*(t),t) - F_{\max} \cdot \frac{\frac{\partial\phi}{\partial\boldsymbol{x}}\big|_{(\boldsymbol{X}_{\boldsymbol{p}}^*(t),t)}}{\left\|\frac{\partial\phi}{\partial\boldsymbol{x}}\big|_{(\boldsymbol{X}_{\boldsymbol{p}}^*(t),t)}\right\|}, \quad (4)$$

that is solved backward in time starting from $\boldsymbol{X}_{\boldsymbol{p}}^*(t = t_f) = \boldsymbol{x}_f$ until $\boldsymbol{X}_{\boldsymbol{p}}^*(0) = \boldsymbol{x}_s$. We note that eq. (4) is the characteristic ODE of the reachability PDE (2) [57, 59, 66, 67].

C. Ocean Modeling Forecasts and Glider Parameters

The forecast currents $\boldsymbol{V}(\boldsymbol{x},t)$ were provided by our large-ensemble forecasting of physical ocean fields, uncertainties, and risks using our MIT MSEAS-PE and ESSE systems [48, 49, 53, 54, 68, 69]. These systems have been employed for realistic simulations and fundamental research in many different regions of the World Ocean [6, 22, 70–74]. The MSEAS-PE can simulate (sub-)mesoscale processes over regional domains with complex geometries and varied interactions using an implicit two-way nesting/tiling scheme [48]. We exercised many of our systems' capabilities during MASTR, including deterministic and ensemble initialization schemes [49, 75, 76], tidal prediction and inversion [77], fast-marching coastal objective analysis [78], subgrid-scale models [34, 79], advanced data assimilation [52, 80], and path planning, reachability, and adaptive sampling [5, 6, 52, 81]. Additional details are in [51].

The gliders were piloted using a 1000 m yo-yo pattern. Accordingly, 0–1000 m depth-averaged currents and horizontal glider velocities of 40 to 50 cm/s (RU38) and 30 to 40 cm/s (SeaGlider 625 and 652 and Stommel) were used for reachability computation, except in special situations [47] and where indicated in the results highlighted next.

III. REAL-TIME FORECASTING FOR GLIDERS

We now highlight some of our MASTR real-time forecasts for guiding glider motions in the dynamic western Caribbean Sea and Gulf of Mexico during February to April 2024 [47]. The forecasts and guidance were issued on our MASTR web-pages, WhatsApp for rapid dissemination, and Zoom team meetings. They included reachability analyses, optimal path planning for glider recovery and gliders in distress, and planning of future glider deployments.

A. Forward Reachability

Throughout the duration of MASTR, we issued daily deterministic reachability forecasts for each of the four gliders operating in the Gulf of Mexico. We numerically integrated the PDE (2) for each glider and for a set of glider maximum propulsion speeds F_{max} (Sects. II-B–II-C). For normal operations, we used the vertically-averaged MSEAS-PE ocean current forecasts as $V(x, t)$.

Figure 1 illustrates one of such forecast of reachability fronts (issued on April 5, 2024), here displayed at 12-hour intervals, with their line thickness increasing for later times. They are overlaid on our MSEAS-PE forecast of the 0-1000 m averaged horizontal current velocity magnitude and vectors, shown at the temporal midpoint of the glider reachability forecast.
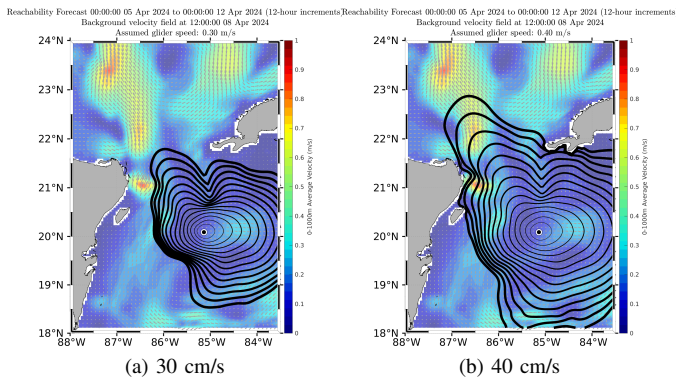

(a) 30 cm/s   (b) 40 cm/s

Fig. 1: Real-time forecast of forward reachability fronts (at 12-hour intervals, increasing thickness for later times) for two different assumed glider speeds (30 and 40 cm/s), overlaid on forecast 0-1000 m averaged currents (m/s) for the Stommel glider, issued on 05 Apr 2024 [47].

The reachability fronts shown are the boundary of the set of locations that the glider can reach within a certain duration, for two different horizontal glider propulsion speed F_{max}: 30 and 40 cm/s. The shape and growth of the reachable front are driven by the glider's horizontal propulsion and the dynamic local currents. Generally, strong northward Loop Current in the Yucatan Current especially on its western side near the Mexican coastline causes the reachable fronts to spread more quickly in that region, especially by Arrowsmith Bank and beyond.

B. Probabilistic Forward Reachability

To account for uncertainties in forecast ocean currents, we computed probabilistic reachability fields using our ESSE ensemble ocean forecasts [51]. First, the reachable set was forecast for each ensemble member (Sect. II-A): the HJB PDE (2) was integrated for each $V(x, t; \omega)$, providing the sample path realizations $\mathcal{R}(x_s, t; \omega)$. Then, the overall probability of the forward reachability field was obtained by taking the union of each member's reachable set: at each finite-volume cell, the number of reachable set realizations with a negative value is counted and the total is normalized by the number of members.

(a) Day 2: Mar 24   (b) Day 3: March 25

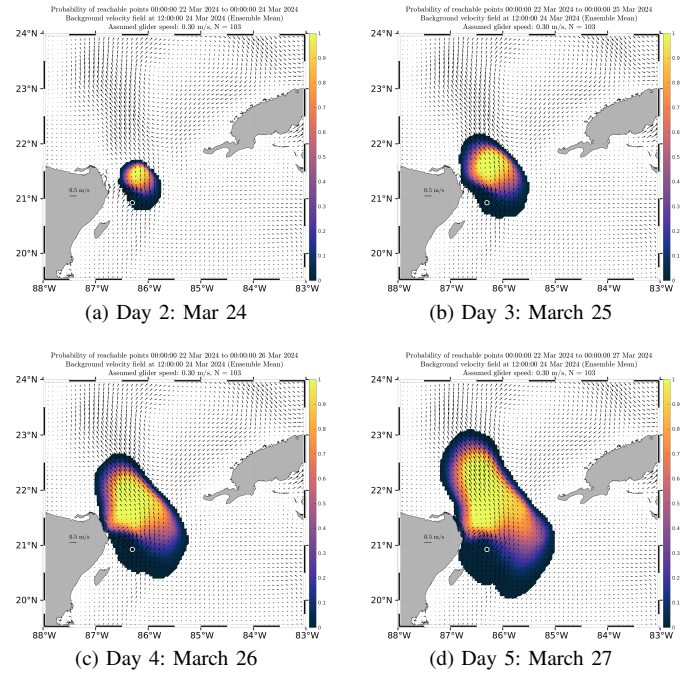(c) Day 4: March 26   (d) Day 5: March 27

Fig. 2: Real-time forecast of probabilistic forward reachability: probability density function (PDF) that a location is reachable after 2, 3, 4, and 5 days by a glider of 0.3 m/s propulsion-speed, starting at the white dot location on 00Z March 22, computed by integrating the HJB PDE (2) for each of the MIT-MSEAS ensemble ocean current forecasts (N=103 members). The PDF field is overlaid on the ensemble mean current vectors forecast at $t = 2.5$ days.

One of such probabilistic reachability forecast (issued on March 22, 2024) for March 22-27, 2024, is shown in Figure 2. The colored field is the forecast probability that a spatial location is within the reachable set of the glider on March 23, 25, and 27 (days 1, 3, and 5 of the forecast). This probability is overlaid on the ensemble mean velocity vectors (at the temporal midpoint of the probabilistic forecast).

These probabilistic forecasts provide additional clarity on which regions are reachable under most current conditions, and which regions are possibly reachable, but only under more extreme currents (e.g., much weaker or stronger, or much different, than normally expected currents). For the example shown in Figure 2, the glider could likely reach many locations to the north through the Yucatan Strait under any current condition (within the expected statistical distribution). However, the probability that the glider could reach locations directly to the south near Cozumel is much lower and would require more extreme currents (in this case, weak northward currents).

Because the deterministic reachability predictions described in Section III-A require that the forecasted velocity field is accurate, this probabilistic approach allows us to quantify the effect of uncertainty in the underlying forecast on reachability predictions. Also, from this probability density field (PDF), we can compute the mean, skewness, kurtosis, and other statistical quantities of the reachability field [51] as well as probabilistic

4

(a) Reachability: March 29–April 5   (b) Reachability: April 2–9   (c) Prob. reachability: April 3–5   (d) Actual track: March 29–April 4
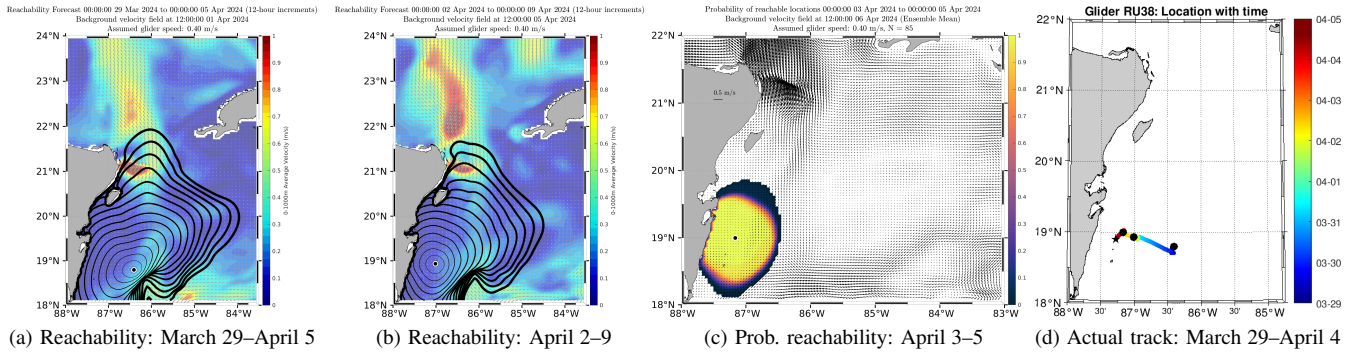
Fig. 3: Real-time forward reachability forecasts for the pickup of glider RU38. (a–b) Reachability fronts at 12-hour intervals, issued March 29 and April 2. The assumed glider speed was 40 cm/s; (c) Probabilistic reachability forecast for April 3–5; (d) Actual track of glider RU38 from March 29 until pickup on April 4. Black dots denote the glider location at 0Z on March 29, April 2, and April 3. The star indicates the pickup location.

risks [62] which can be most useful for glider operators.

C. Reachability and Path Planning for Glider Pickup

Reachability and path planning forecasts were also used to assist in the pickup of gliders at the end of their missions.

For the recovery of glider RU38, we had to contend with the competing issues of arranging for a boat and crew for the recovery versus depleting batteries. The operators chose to move the glider into a region of low velocity. The MSEAS reachability forecasts were used to assess how likely the glider could remain in the area. The forecast issued on March 29 (Fig. 3a) shows extensions to both the north and south due to the splitting of a westward-flowing current between $18°N$ and $18.5°N$ as it impinges on the continental shelf. The starting point of the glider is within the splitting current, suggesting that the glider should head inshore. Forecasts issued on April 2 (deterministic, Fig. 3b) and April 3 (probabilistic, Fig. 3c) show that the splitting of the westward current is still extending the reachability to the north and south. The probabilistic forecast shows that the glider can reach the pickup location with a probability near 1. The actual path of glider RU38 is shown in Fig. 3(d). It confirms the skill of the reachability forecasts as the actual path is fully contained within them.

The MSEAS forecasting for the recovery of glider Stommel began on April 5 (Fig. 4a). That reachability forecast issued on April 5, 2024 indicated that it would be possible to reach the desired pickup location by April 15 if a circuitous trajectory were used to take advantage of a favorable forecast anticyclonic circulation to the west and south, along the optimal path (Fig. 4a). To follow this optimal path, one needs to choose vehicle headings (red arrows, Fig. 4b) that account for the currents (blue arrows, Fig. 4b) to achieve the resultant trajectories that lie along the optimal path (green arrows, Fig. 4b). These optimal vehicle headings are summarized in the polar diagram (Fig. 4c). The operator instead opted for a more traditional straight-line path. On April 9 a new forecast based on the new Stommel position was issued (Fig. 4d). With this new position, the optimal path is closer to the straight line, although the initial heading is due south instead of directly to

the pickup point, indicating that there were still some benefits to extract from the currents. The MSEAS reachability forecast and time-optimal path now predicted an April 17 pickup date from that new start position, if the optimal headings were followed. The actual track (Fig. 4e) led to an April 20 pickup. We note that this sub-optimal path remained contained within the forecast reachability fronts.

D. Time-Optimal Paths and Recovery for Gliders in Distress

Reachability forecasts were also provided in real time to assist in the localization and retrieval of gliders in distress. In these cases, the glider model was modified in real time to represent the real glider. For example, some glider motions were modeled predominantly due to advection with surface currents. Other gliders had limited motions and were affected only by currents at specific depths or were assumed to be attempting station-keeping and could oppose a specified current speed [47].

We first consider a localization example. On March 17, SG652 began to malfunction near the Yucatán Strait (a damaged wing was suspected, evidenced by difficulty controlling roll and slower horizontal speeds). The glider was assumed to be diving/rising between 0 and 1000 m without generating significant horizontal thrust (effectively drifting with the currents, starting within a circle of uncertainty). This malfunction occurred when the glider was just east of the LC entering into the GoM and just west of the Cuban EEZ. This raised questions as to whether the glider was in danger of (a) being swept northward by the LC or (b) drifting into Cuban waters.

We issued a reachability forecast on March 27, 2024 initialized the last known position of SG652 and evolved the front forward in time, using a speed of 5 cm/s (instead of the nominal speeds of 30 to 40 cm/s) to account for uncertainty in both the glider and forecast current speeds (Fig. 5). Over the 6-day forecast period, we forecasted that the reachability front was advected around the smaller, slow anticyclonic gyre, remaining near the initial point but avoiding the Cuban waters and only brushing the edges of the LC inflow. These results gave the glider operators confidence that they could continue

(a) Reachability: April 5–15   (b) Optimal path and controls: April 5–15   (c) Optimal headings: April 5–15

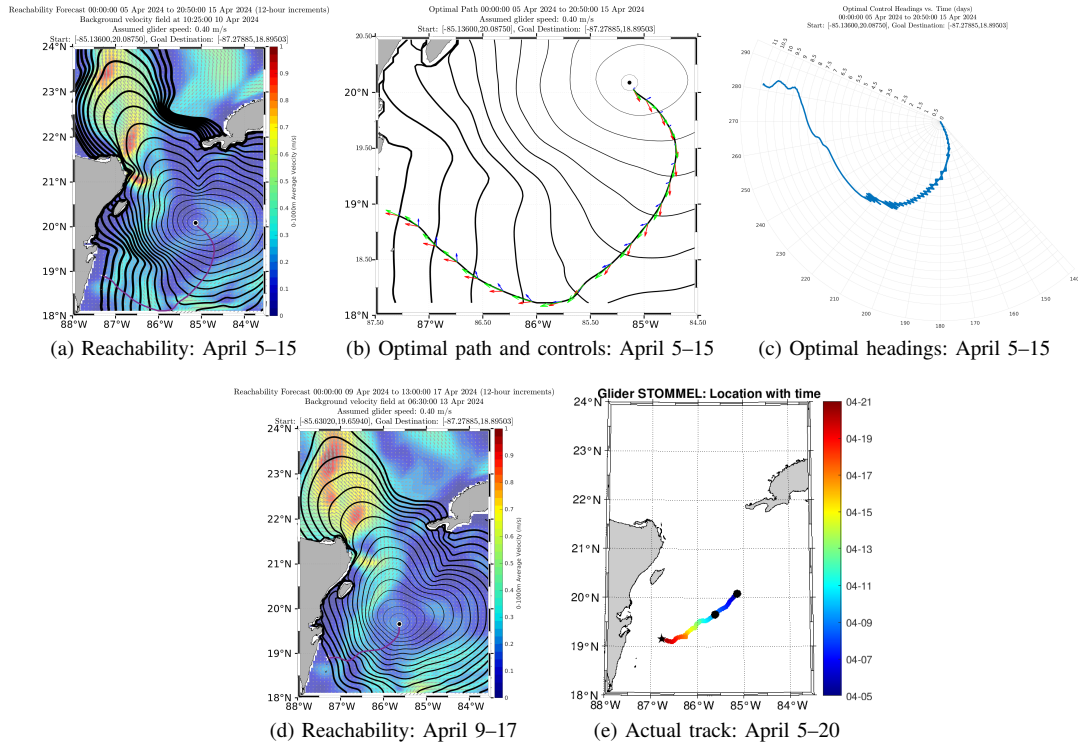(d) Reachability: April 9–17   (e) Actual track: April 5–20

Fig. 4: Long-range forward reachability forecasts for the pickup of glider Stommel. (a,d) Reachability front forecasts at 12-hour intervals, issued April 5 and April 9. The assumed glider speed was 40 cm/s; (b) Optimal path for April 5–15, with forecast current (blue), optimal vehicle propulsion (red), and net total velocity (green) vectors, overlaid on reachability fronts; (c) Optimal heading angles for April 5–15; (e) Actual track of Stommel from April 5 until pickup on April 20. The black dots indicate the glider location at 0Z on April 5 and April 9. The star indicates the pickup location.
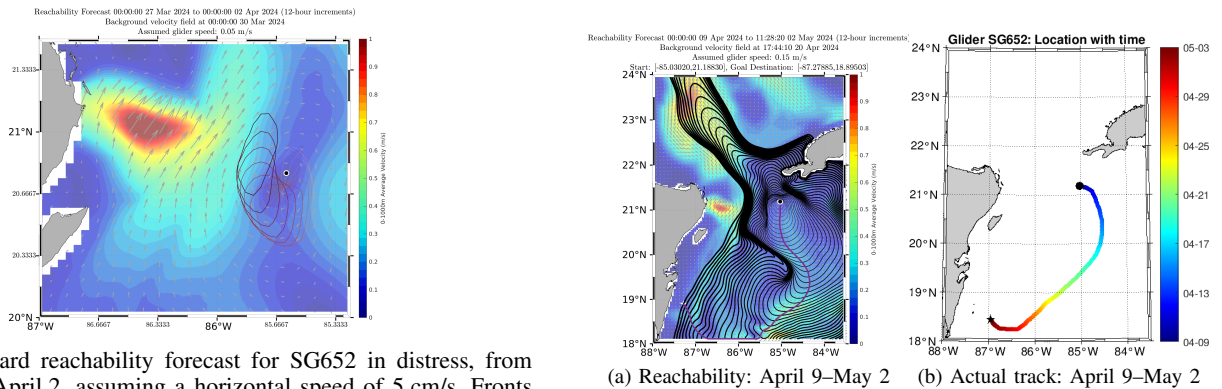

Fig. 5: Forward reachability forecast for SG652 in distress, from March 27 to April 2, assuming a horizontal speed of 5 cm/s. Fronts are plotted every 6 hours, and colored by time with darker, thicker lines representing later times.

(a) Reachability: April 9–May 2   (b) Actual track: April 9–May 2

Fig. 6: Long-range forward reachability forecasts for the pickup of SG652. (a) Reachability front forecasts at 12-hour intervals, issued April 9. The assumed glider speed was 15 cm/s; (b) Actual track of SG652 from April 9 until pickup on May 2. The black dot indicates the glider location at 0Z on April 9. The star indicates the pickup location.

testing their malfunctioning glider in this area. After the testing was completed, it was time to plan for the recovery of SG652.

On April 9, we provided a long-range forecast of the reachability sets and time-optimal path for the planned recovery of SG652, assuming a glider speed of 15 cm/s, near the coast of Quintana Roo (Fig. 6a). The optimal path again takes advantage of the anticyclonic circulation to the south and west, arriving at the pickup point by May 2. The operators of SG652 also chose to take advantage of this circulation and were able to also reach the pick-up point by May 2 (Fig. 6b). Again, the forecast reachability front contains the actual glider path.

E. Glider Deployment Planning

Finally, we investigated the use our reachability forecasting to explore the feasibility of launching gliders from US waters and traveling to the Yucatán Channel, rather than transporting everything to Mexico. When considering locations for glider
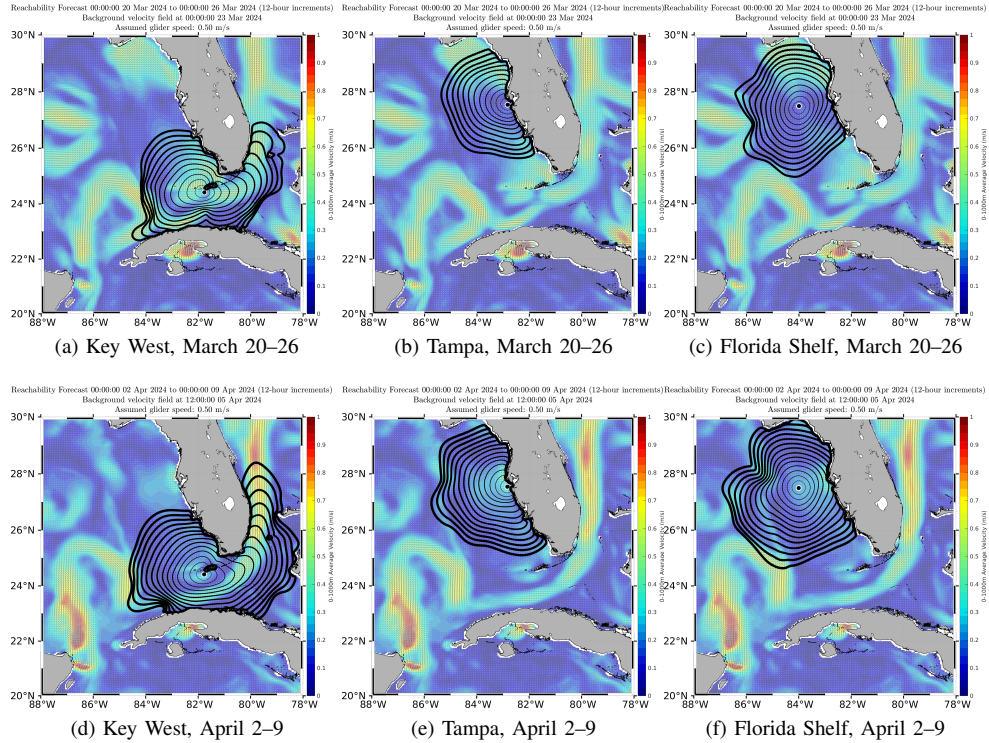
Fig. 7: Reachability front forecasts (black lines) every 12 hours for virtual gliders starting from several potential deployment locations. In all cases, the assumed glider speed was 50 cm/s. (a–c) Forecasts for March 20–26; (d–f) Forecasts for April 2–9.

deployment, a cost-benefit analysis is considered between travel time, deployment vessel cost, and glider battery life. To initiate that study, we issued several forecasts of reachability for virtual deployments from Key West, Tampa and offshore from Tampa [47].

Figure 7 shows two virtual reachability forecasts issued on March 20 and April 2, 2024 (i.e., separated by about 2 weeks). During this period, the basic LC state is unchanged but some smaller scale details have evolved. This is reflected in the reachability forecasts. In both cases, the virtual glider launches from Key West have experienced 1-2 days of helpful currents and are within a day or two from the Yucatán Channel (with the March 20-26 being a bit further along). The reachability forecasts indicate that great care would be needed to ensure that the gliders would not be swept up in the LC/Gulf Stream and advected out of the GOM. In both cases, the Florida Shelf releases have just barely reached the LC for an assist and are probably about 3-4 days behind the Key West releases. Finally, the Tampa releases are about 2-3 days away from the LC and hence 2-3 days behind the Florida Shelf releases.

IV. CONCLUSIONS

In this paper, we described the governing differential equations to produce exact solutions for time-optimal path planning and reachability analysis for both deterministic and probabilistic conditions. We applied these equations for deterministic and probabilistic forecasts in real-time during the MASTR experiment [44, 47]. We demonstrated that the actual paths of gliders in the water were contained within our reachable set forecasts and even in accord with the dynamic evolution of the reachability fronts. Our forecasts of time-optimal headings and paths also explained real glider motions, even for longer-range predictions of weeks to a month duration. Reachability and time-optimal path planning forecasts were successfully employed for glider recovery and gliders in distress. They also enabled exploring options for future glider deployments We note that these reachability forecasts, along with uncertainty forecasts [47, 51], were not just intellectual exercises but were used in real-time by the glider operators to achieve their mission. This confirms that principled optimal path planning is not only feasible in real time but is also an important tool for operations.

Future optimal path-planning and reachability missions will include experiments with other real autonomous ocean vehicles [41, 42], more complex operations with multi-vehicles and coordinated teams [63, 82, 83], and onboard implementations so that vehicles can directly predict their optimal controls [84–86]. The inclusion of hazard modeling and high altitude drones and small satellites would be beneficial [83, 87, 88], and could include probabilistic hazards and risks modeling [61, 62, 89], leading to stochastic hazard-time path planning. Finally, multi-time and multi-field reachability will be useful in many applications including efficient capabilities for frequent re-planning [57, 90, 91].

REFERENCES

[1] Z. Zeng, L. Lian, K. Sammut, F. He, Y. Tang, and A. Lammas, "A survey on path planning for persistent autonomy of autonomous underwater vehicles," *Ocean Engineering*, vol. 110, pp. 303–313, 2015.

[2] J. J. Leonard and A. Bahr, *Autonomous Underwater Vehicle Navigation*. Cham: Springer International Publishing, 2016, pp. 341–358.

[3] D. Kularatne, S. Bhattacharya, and M. A. Hsieh, "Time and energy optimal path planning in general flows." in *Robotics: Science and Systems*, 2016.

[4] Z. Zeng *et al.*, "A comparison of optimization techniques for auv path planning in environments with ocean currents," *Robotics and Autonomous Systems*, vol. 82, pp. 61–72, 2016.

[5] P. F. J. Lermusiaux, T. Lolla, P. J. Haley, Jr., K. Yigit, M. P. Ueckermann, T. Sondergaard, and W. G. Leslie, "Science of autonomy: Time-optimal path planning and adaptive sampling for swarms of ocean vehicles," in *Springer Handbook of Ocean Engineering: Autonomous Ocean Vehicles, Subsystems and Control*, T. Curtin, Ed. Springer, 2016, ch. 21, pp. 481–498.

[6] P. F. J. Lermusiaux, D. N. Subramani, J. Lin, C. S. Kulkarni, A. Gupta, A. Dutt, T. Lolla, P. J. Haley, Jr., W. H. Ali, C. Mirabito, and S. Jana, "A future for intelligent autonomous ocean observing systems," *Journal of Marine Research*, vol. 75, no. 6, pp. 765–813, Nov. 2017, the Sea. Volume 17, The Science of Ocean Prediction, Part 2.

[7] D. Li, P. Wang, and L. Du, "Path planning technologies for autonomous underwater vehicles-a review," *IEEE Access*, vol. 7, pp. 9745–9768, 2018.

[8] B. Patle, A. Pandey, D. Parhi, A. Jagadeesh *et al.*, "A review: On path planning strategies for navigation of mobile robot," *Defence Technology*, vol. 15, no. 4, pp. 582–606, 2019.

[9] J. R. Sanchez-Ibanez, C. J. Pérez-del Pulgar, and A. García-Cerezo, "Path planning for autonomous mobile robots: A review," *Sensors*, vol. 21, no. 23, p. 7898, 2021.

[10] C. Cheng, Q. Sha, B. He, and G. Li, "Path planning and obstacle avoidance for auv: A review," *Ocean Engineering*, vol. 235, p. 109355, 2021.

[11] T. B. Curtin, J. G. Bellingham, J. Catipovic, and D. Webb, "Autonomous oceanographic sampling networks," *Oceanography*, vol. 6, no. 3, pp. 86–94, 1993.

[12] H. Schmidt *et al.*, "Real-time frontal mapping with AUVs in a coastal environment," in *OCEANS 96 MTS/IEEE Conference Proceedings. The Coastal Ocean-Prospects for the 21st Century*, vol. 3. IEEE, 1996, pp. 1094–1098.

[13] J. Xu, P. F. J. Lermusiaux, P. J. Haley Jr., W. G. Leslie, and O. G. Logutov, "Spatial and Temporal Variations in Acoustic propagation during the PLUSNet-07 Exercise in Dabob Bay," in *Proceedings of Meetings on Acoustics (POMA)*, vol. 4. Acoustical Society of America 155th Meeting, 2008, p. 11.

[14] Argo, "Argo float data and metadata from Global Data Assembly Centre (Argo GDAC)," 2000.

[15] G. Griffiths, *Technology and applications of autonomous underwater vehicles*. CRC Press, 2002, vol. 2.

[16] D. M. Crimmins *et al.*, "Long-endurance test results of the solar-powered AUV system," in *OCEANS 2006*. IEEE, 2006, pp. 1–5.

[17] O. Schofield, S. Glenn, J. Orcutt, M. Arrott, M. Meisinger, A. Gangopadhyay, W. Brown, R. Signell, M. Moline, Y. Chao, S. Chien, D. Thompson, A. Balasuriya, P. F. J. Lermusiaux, and M. Oliver, "Automated sensor networks to advance ocean science," *Eos Trans. AGU*, vol. 91, no. 39, pp. 345–346, Sep. 2010.

[18] J. Yuh, "Design and control of autonomous underwater robots: A survey," *Autonomous Robots*, vol. 8, no. 1, pp. 7–24, 2000.

[19] J. G. Bellingham and K. Rajan, "Robotics in remote and hostile environments," *Science*, vol. 318, no. 5853, pp. 1098–1102, 2007.

[20] D. C. Webb, P. J. Simonetti, and C. P. Jones, "Slocum: An underwater glider propelled by environmental energy," *IEEE Journal of oceanic engineering*, vol. 26, no. 4, pp. 447–452, 2001.

[21] S. R. Ramp, R. E. Davis, N. E. Leonard, I. Shulman, Y. Chao, A. R. Robinson, J. Marsden, P. F. J. Lermusiaux, D. M. Fratantoni, J. D. Paduan, F. P. Chavez, F. L. Bahr, S. Liang, W. Leslie, and Z. Li, "Preparing to predict: The second Autonomous Ocean Sampling Network (AOSN-II) experiment in the Monterey Bay," *Deep Sea Research Part II: Topical Studies in Oceanography*, vol. 56, no. 3–5, pp. 68–86, Feb. 2009.

[22] P. J. Haley, Jr., P. F. J. Lermusiaux, A. R. Robinson, W. G. Leslie, O. Logoutov, G. Cossarini, X. S. Liang, P. Moreno, S. R. Ramp, J. D. Doyle, J. Bellingham, F. Chavez, and S. Johnston, "Forecasting and reanalysis in the Monterey Bay/California Current region for the Autonomous Ocean Sampling Network-II experiment," *Deep Sea Research Part II: Topical Studies in Oceanography*, vol. 56, no. 3–5, pp. 127–148, Feb. 2009.

[23] N. E. Leonard *et al.*, "Coordinated control of an underwater glider fleet in an adaptive ocean sampling field experiment in Monterey Bay," *Journal of Field Robotics*, vol. 27, no. 6, pp. 718–740, 2010.

[24] S. Glenn *et al.*, "The trans-Atlantic Slocum glider expeditions: A catalyst for undergraduate participation in ocean science and technology," *Marine Technology Society Journal*, vol. 45, no. 1, pp. 52–67, 2011.

[25] R. N. Smith *et al.*, "Persistent ocean monitoring with underwater gliders: Adapting sampling resolution," *Journal of Field Robotics*, vol. 28, no. 5, pp. 714–741, 2011.

[26] A. Stuntz, J. S. Kelly, and R. N. Smith, "Enabling persistent autonomy for underwater gliders with ocean model predictions and terrain-based navigation," *Frontiers in Robotics and AI*, vol. 3, p. 23, 2016.

[27] C. S. Kulkarni and P. F. J. Lermusiaux, "Three-dimensional time-optimal path planning in the ocean," *Ocean Modelling*, vol. 152, Aug. 2020.

[28] R. Zhang, B. He, Y. Wang, W. Ma, and S. Yang, "Recent advances in path planning for underwater gliders: A comprehensive review," *Ocean Engineering*, vol. 299, p. 117166, 2024.

[29] H. Hu, Z. Zhang, T. Wang, and X. Peng, "Underwater glider 3D path planning with adaptive segments and optimal motion parameters based on improved JADE algorithm," *Ocean Engineering*, vol. 299, p. 117377, 2024.

[30] D. L. Rudnick, "Ocean research enabled by underwater gliders," *Annual review of marine science*, vol. 8, no. 1, pp. 519–541, 2016.

[31] T. N. Miles, D. Zhang, G. R. Foltz, J. A. Zhang, C. Meinig, F. Bringas, J. Triñanes, M. Le Hénaff, M. F. A. Vargas, S. Coakley *et al.*, "Uncrewed ocean gliders and saildrones support

hurricane forecasting and research," *Oceanography*, vol. 34, no. 4, pp. 78–81, 2021.

[32] N. von Oppeln-Bronikowski, B. de Young, M. Belzile, A. Comeau, F. Cyr, R. Davis, P. Emery, C. Richards, D. Hebert, and J. Van Der Meer, "Best practices for operating underwater gliders in atlantic canada," *Frontiers in Marine Science*, vol. 10, p. 1108326, 2023.

[33] P. F. J. Lermusiaux, C.-S. Chiu, G. G. Gawarkiewicz, P. Abbot, A. R. Robinson, R. N. Miller, P. J. Haley, Jr, W. G. Leslie, S. J. Majumdar, A. Pang, and F. Lekien, "Quantifying uncertainties in ocean predictions," *Oceanography*, vol. 19, no. 1, pp. 92–105, 2006.

[34] P. F. J. Lermusiaux, "Uncertainty estimation and prediction for interdisciplinary ocean dynamics," *Journal of Computational Physics*, vol. 217, no. 1, pp. 176–199, 2006.

[35] C. D. Haldeman, D. K. Aragon, T. Miles, S. M. Glenn, and A. G. Ramos, "Lessening biofouling on long-duration AUV flights: Behavior modifications and lessons learned," in *OCEANS 2016 MTS/IEEE Monterey*. IEEE, 2016, pp. 1–8.

[36] X. Chen, N. Bose, M. Brito, F. Khan, B. Thanyamanta, and T. Zou, "A review of risk analysis research for the operations of autonomous underwater vehicles," *Reliability Engineering & System Safety*, vol. 216, p. 108011, 2021.

[37] D. L. Rudnick, R. E. Davis, C. C. Eriksen, D. M. Fratantoni, and M. J. Perry, "Underwater gliders for ocean research," *Marine Technology Society Journal*, vol. 38, no. 2, pp. 73–84, 2004.

[38] L. M. Ware, "Design of control for efficiency of AUV power systems; design of control for efficiency of autonomous underwater vehicle power systems," Ph.D. dissertation, MIT, 2012.

[39] N. B. Pulsone, D. P. Hart, A. M. Siegel, J. R. Edwards, and K. E. Railey, "Aluminum-water energy system for autonomous undersea vehicles," *Lincoln Laboratory Journal*, vol. 22, no. 2, pp. 79–90, 2017.

[40] P. Godart, J. Fischman, and D. Hart, "Kilowatt-scale fuel cell systems powered by recycled aluminum," *Journal of Electrochemical Energy Conversion and Storage*, vol. 18, no. 1, 2021.

[41] D. N. Subramani, P. F. J. Lermusiaux, P. J. Haley, Jr., C. Mirabito, S. Jana, C. S. Kulkarni, A. Girard, D. Wickman, J. Edwards, and J. Smith, "Time-optimal path planning: Real-time sea exercises," in *Oceans '17 MTS/IEEE Conference*, Aberdeen, Jun. 2017.

[42] P. F. J. Lermusiaux, P. J. Haley, Jr., S. Jana, A. Gupta, C. S. Kulkarni, C. Mirabito, W. H. Ali, D. N. Subramani, A. Dutt, J. Lin, A. Shcherbina, C. Lee, and A. Gangopadhyay, "Optimal planning and sampling predictions for autonomous and Lagrangian platforms and sensors in the northern Arabian Sea," *Oceanography*, vol. 30, no. 2, pp. 172–185, Jun. 2017, special issue on Autonomous and Lagrangian Platforms and Sensors (ALPS).

[43] L. R. Centurioni *et al.*, "Northern Arabian Sea circulation-autonomous research (NASCar): A research initiative based on autonomous sensors," *Oceanography*, vol. 30, no. 2, pp. 74–87, Jun. 2017, special issue on Autonomous and Lagrangian Platforms and Sensors (ALPS).

[44] S. F. DiMarco *et al.*, "Applications of adaptive sampling strategies of autonomous vehicles, drifters, floats, and HF-radar, to improve Loop Current system dynamics forecasts in the deepwater Gulf of Mexico," in *Offshore Technology Conference*. OTC, 2023, p. D031S035R005.

[45] A. Knap *et al.*, "Understanding the Gulf Ocean System program: Informing stakeholders and improving prediction of the Loop Current system using advanced observational and numerical tools," in *Offshore Technology Conference*. OTC, 2023, p. D031S035R004.

[46] T. Lolla, M. P. Ueckermann, K. Yiğit, P. J. Haley, Jr., and P. F. J. Lermusiaux, "Path planning in time dependent flow fields using level set methods," in *IEEE International Conference on Robotics and Automation (ICRA), 14-18 May 2012*, 2012, pp. 166–173.

[47] MSEAS MASTR Ex., "MASTR Real-time Gulf of Mexico Sea Experiment 2024: Gulf of Mexico – February–April, 2024," Apr. 2024. [Online]. Available: http://mseas.mit.edu/Sea_exercises/GOFFISH/MASTR/

[48] P. J. Haley, Jr. and P. F. J. Lermusiaux, "Multiscale two-way embedding schemes for free-surface primitive equations in the "Multidisciplinary Simulation, Estimation and Assimilation System"," *Ocean Dynamics*, vol. 60, no. 6, pp. 1497–1537, Dec. 2010.

[49] P. J. Haley, Jr., A. Agarwal, and P. F. J. Lermusiaux, "Optimizing velocities and transports for complex coastal regions and archipelagos," *Ocean Modelling*, vol. 89, pp. 1–28, May 2015.

[50] P. J. Haley, Jr., C. Mirabito, M. Doshi, and P. F. J. Lermusiaux, "Ensemble forecasting for the Gulf of Mexico Loop Current region," in *OCEANS 2023 IEEE/MTS Gulf Coast*. Biloxi, MS: IEEE, Sep. 2023.

[51] P. F. J. Lermusiaux, P. J. Haley, Jr., C. Mirabito, E. M. Mule *et al.*, "Real-time ocean probabilistic forecasts, reachability analysis, and adaptive sampling in the Gulf of Mexico," in *OCEANS 2024 IEEE/MTS Halifax*. Halifax: IEEE, Sep. 2024, in press.

[52] P. F. J. Lermusiaux, "Adaptive modeling, adaptive data assimilation and adaptive sampling," *Physica D: Nonlinear Phenomena*, vol. 230, no. 1, pp. 172–196, 2007.

[53] P. F. J. Lermusiaux, P. J. Haley, W. G. Leslie, A. Agarwal, O. Logutov, and L. J. Burton, "Multiscale physical and biological dynamics in the Philippine Archipelago: Predictions and processes," *Oceanography*, vol. 24, no. 1, pp. 70–89, 2011, Special Issue on the Philippine Straits Dynamics Experiment.

[54] P. F. J. Lermusiaux, C. Mirabito, P. J. Haley, Jr., W. H. Ali, A. Gupta, S. Jana, E. Dorfman, A. Laferriere, A. Kofford, G. Shepard, M. Goldsmith, K. Heaney, E. Coelho, J. Boyle, J. Murray, L. Freitag, and A. Morozov, "Real-time probabilistic coupled ocean physics-acoustics forecasting and data assimilation for underwater GPS," in *OCEANS 2020 IEEE/MTS*. IEEE, Oct. 2020, pp. 1–9.

[55] T. Lolla, P. F. J. Lermusiaux, M. P. Ueckermann, and P. J. Haley, Jr., "Time-optimal path planning in dynamic flows using level set equations: Theory and schemes," *Ocean Dynamics*, vol. 64, no. 10, pp. 1373–1397, 2014.

[56] S. Bansal, M. Chen, S. Herbert, and C. J. Tomlin, "Hamilton-Jacobi reachability: A brief overview and recent advances," in *2017 IEEE 56th Annual Conference on Decision and Control (CDC)*. IEEE, 2017, pp. 2242–2253.

[57] M. M. Doshi, M. S. Bhabra, and P. F. J. Lermusiaux, "Energy-time optimal path planning in dynamic flows: Theory and schemes," *Computer Methods in Applied Mechanics and Engineering*, vol. 405, p. 115865, Feb. 2023.

[58] S. V. T. Lolla, "Path planning and adaptive sampling in the coastal ocean," Ph.D. dissertation, Massachusetts Institute of Technology, Department of Mechanical Engineering, Cambridge, Massachusetts, Feb. 2016.

[59] T. Lolla and P. F. J. Lermusiaux, "A forward reachability equation for minimum-time path planning in strong dynamic flows," Department of Mechanical Engineering, Massachusetts Institute of Technology, Cambridge, MA, USA, MSEAS Report 27, 2017.

[60] A. H. Jazwinski, *Stochastic processes and filtering theory*. Courier Corporation, 2007.

[61] D. N. Subramani, Q. J. Wei, and P. F. J. Lermusiaux, "Stochastic time-optimal path-planning in uncertain, strong, and dynamic flows," *Computer Methods in Applied Mechanics and Engineering*, vol. 333, pp. 218–237, 2018.

[62] D. N. Subramani and P. F. J. Lermusiaux, "Risk-optimal path planning in stochastic dynamic environments," *Computer Meth-*

9

ods in Applied Mechanics and Engineering, vol. 353, pp. 391–415, Aug. 2019.

[63] T. Lolla, P. J. Haley, Jr., and P. F. J. Lermusiaux, "Path planning in multiscale ocean flows: Coordination and dynamic obstacles," *Ocean Modelling*, vol. 94, pp. 46–66, 2015.

[64] W. H. Ali, A. Charous, C. Mirabito, P. J. Haley, Jr., and P. F. J. Lermusiaux, "MSEAS-ParEq for ocean-acoustic modeling around the globe," in *OCEANS 2023 IEEE/MTS Gulf Coast*. Biloxi, MS: IEEE, Sep. 2023.

[65] W. H. Ali and P. F. J. Lermusiaux, "Dynamically orthogonal narrow-angle parabolic equations for stochastic underwater sound propagation. part I: Theory and schemes," *Journal of the Acoustical Society of America*, vol. 155, no. 1, pp. 640–655, Jan. 2024.

[66] F. Feppon and P. F. J. Lermusiaux, "Dynamically orthogonal numerical schemes for efficient stochastic advection and Lagrangian transport," *SIAM Review*, vol. 60, no. 3, pp. 595–625, 2018.

[67] C. S. Kulkarni and P. F. J. Lermusiaux, "Advection without compounding errors through flow map composition," *Journal of Computational Physics*, vol. 398, p. 108859, Dec. 2019.

[68] P. F. J. Lermusiaux and A. R. Robinson, "Data assimilation via Error Subspace Statistical Estimation, part I: Theory and schemes," *Monthly Weather Review*, vol. 127, no. 7, pp. 1385–1407, 1999.

[69] P. F. J. Lermusiaux, "Data assimilation via Error Subspace Statistical Estimation, part II: Mid-Atlantic Bight shelfbreak front simulations, and ESSE validation," *Monthly Weather Review*, vol. 127, no. 7, pp. 1408–1432, Jul. 1999.

[70] W. G. Leslie, A. R. Robinson, P. J. Haley, Jr, O. Logutov, P. A. Moreno, P. F. J. Lermusiaux, and E. Coelho, "Verification and training of real-time forecasting of multi-scale ocean dynamics for maritime rapid environmental assessment," *Journal of Marine Systems*, vol. 69, no. 1, pp. 3–16, 2008.

[71] D. N. Subramani, P. J. Haley, Jr., and P. F. J. Lermusiaux, "Energy-optimal path planning in the coastal ocean," *Journal of Geophysical Research: Oceans*, vol. 122, pp. 3981–4003, 2017.

[72] C. S. Kulkarni, P. J. Haley, Jr., P. F. J. Lermusiaux, A. Dutt, A. Gupta, C. Mirabito, D. N. Subramani, S. Jana, W. H. Ali, T. Peacock, C. M. Royo, A. Rzeznik, and R. Supekar, "Real-time sediment plume modeling in the Southern California Bight," in *OCEANS Conference 2018*. Charleston, SC: IEEE, Oct. 2018.

[73] A. Gupta, P. J. Haley, D. N. Subramani, and P. F. J. Lermusiaux, "Fish modeling and Bayesian learning for the Lakshadweep Islands," in *OCEANS 2019 MTS/IEEE SEATTLE*. Seattle: IEEE, Oct. 2019, pp. 1–10.

[74] P. F. J. Lermusiaux, M. Doshi, C. S. Kulkarni, A. Gupta, P. J. Haley, Jr., C. Mirabito, F. Trotta, S. J. Levang, G. R. Flierl, J. Marshall, T. Peacock, and C. Noble, "Plastic pollution in the coastal oceans: Characterization and modeling," in *OCEANS 2019 MTS/IEEE SEATTLE*. Seattle: IEEE, Oct. 2019, pp. 1–10.

[75] P. F. J. Lermusiaux, D. G. M. Anderson, and C. J. Lozano, "On the mapping of multivariate geophysical fields: Error and variability subspace estimates," *Quarterly Journal of the Royal Meteorological Society*, vol. 126, no. 565, pp. 1387–1429, 2000.

[76] P. F. J. Lermusiaux, "On the mapping of multivariate geophysical fields: Sensitivities to size, scales, and dynamics," *Journal of Atmospheric and Oceanic Technology*, vol. 19, no. 10, pp. 1602–1637, 2002.

[77] O. G. Logutov and P. F. J. Lermusiaux, "Inverse barotropic tidal estimation for regional ocean applications," *Ocean Modelling*, vol. 25, no. 1–2, pp. 17–34, 2008. [Online]. Available: http://www.sciencedirect.com/science/article/pii/S1463500308000851

[78] A. Agarwal and P. F. J. Lermusiaux, "Statistical field estimation for complex coastal regions and archipelagos," *Ocean Modelling*, vol. 40, no. 2, pp. 164–189, 2011.

[79] P. F. J. Lermusiaux, "Evolving the subspace of the three-dimensional multiscale ocean variability: Massachusetts Bay," *Journal of Marine Systems*, vol. 29, no. 1, pp. 385–422, 2001.

[80] ——, "Estimation and study of mesoscale variability in the Strait of Sicily," *Dynamics of Atmospheres and Oceans*, vol. 29, no. 2, pp. 255–303, 1999.

[81] P. F. J. Lermusiaux, P. J. Haley, Jr, and N. K. Yilmaz, "Environmental prediction, path planning and adaptive sampling: Sensing and modeling for efficient ocean monitoring, management and pollution control," *Sea Technology*, vol. 48, no. 9, pp. 35–38, 2007.

[82] K. Rajan, F. Aguado, P. Lermusiaux, J. B. de Sousa, A. Subramaniam, and J. Tintore, "METEOR: A Mobile (portable) ocEan roboTic obsErvatORy," *Marine Technology Society Journal*, vol. 55, no. 3, pp. 74–75, May 2021.

[83] B. Schnitzler, P. J. Haley, Jr., C. Mirabito, E. M. Mule, J.-M. Moschetta, D. Delahaye, A. Drouin, and P. F. J. Lermusiaux, "Hazard-time optimal path planning for collaborative air and sea drones," in *OCEANS 2024 IEEE/MTS Halifax*. Halifax: IEEE, Sep. 2024, in press.

[84] J. P. Heuss, P. J. Haley, Jr., C. Mirabito, E. Coelho, M. C. Schönau, K. Heaney, and P. F. J. Lermusiaux, "Reduced order modeling for stochastic prediction onboard autonomous platforms at sea," in *OCEANS 2020 IEEE/MTS*. IEEE, Oct. 2020, pp. 1–10.

[85] T. Ryu, J. P. Heuss, P. J. Haley, Jr., C. Mirabito, E. Coelho, P. Hursky, M. C. Schönau, K. Heaney, and P. F. J. Lermusiaux, "Adaptive stochastic reduced order modeling for autonomous ocean platforms," in *OCEANS 2021 IEEE/MTS*. IEEE, Sep. 2021, pp. 1–9.

[86] T. Ryu, W. H. Ali, P. J. Haley, Jr., C. Mirabito, A. Charous, and P. F. J. Lermusiaux, "Incremental low-rank dynamic mode decomposition model for efficient dynamic forecast dissemination and onboard forecasting," in *OCEANS 2022 IEEE/MTS*. Hampton Roads, VA: IEEE, Oct. 2022, pp. 1–8.

[87] M. Tieppo, E. Pereira, L. González Garcia, M. Rolim, E. Castanho, A. Matos, A. Silva, B. Ferreira, M. Pascoal, E. Almeida, F. Costa, F. Zabel, J. Faria, J. Azevedo, J. Alves, J. Moutinho, L. Gonçalves, M. Martins, N. Cruz, N. Abreu, P. Silva, R. Viegas, S. Jesus, T. Chen, T. Miranda, A. Papalia, D. Hart, J. Leonard, M. Haji, O. de Weck, P. Godart, and P. Lermusiaux, "Submarine cables as precursors of persistent systems for large scale oceans monitoring and autonomous underwater vehicles operation," in *OCEANS 2022 IEEE/MTS*. Hampton Roads, VA: IEEE, Oct. 2022, pp. 1–7.

[88] E. Pereira, M. Tieppo, J. a. Faria, D. Hart, P. Lermusiaux, and The K2D Project Team, "Subsea cables as enablers of a next generation global ocean sensing system," *Oceanography*, vol. 36, no. Supp. 1, Feb. 2023, special issue: "Frontiers in Ocean Observing: Emerging Technologies for Understanding and Managing a Changing Ocean".

[89] A. Doering, M. Wiggert, H. Krasowski, M. Doshi, P. F. J. Lermusiaux, and C. J. Tomlin, "Stranding risk for underactuated vessels in complex ocean currents: Analysis and controllers," in *2023 IEEE 62nd Conference on Decision and Control (CDC)*. Singapore: IEEE, Dec. 2023.

[90] M. Doshi, M. Bhabra, M. Wiggert, C. J. Tomlin, and P. F. J. Lermusiaux, "Hamilton–Jacobi multi-time reachability," in *2022 IEEE 61st Conference on Decision and Control (CDC)*, Cancún, Mexico, Dec. 2022, pp. 2443–2450.

[91] M. S. Bhabra, M. Doshi, and P. F. J. Lermusiaux, "Harvest-time optimal path planning in dynamic flows," 2024, in preparation.